Electrochemical Self-Assembly of Alkanethiolate Molecules on Ni(111) and Polycrystalline Ni Surfaces

Silvina Bengió,[†] Mariano Fonticelli,[†] Guillermo Benítez,[†] Alberto Hernández Creus,[‡] Pilar Carro,[‡] Hugo Ascolani,[§] Guillermo Zampieri,[§] Bárbara Blum,[†] and Roberto C. Salvarezza*[,†]

Instituto de Investigaciones Fisicoquímicas Teóricas y Aplicadas (INIFTA), Universidad Nacional de La Plata, CONICET, Sucursal 4 Casilla de Correo 16, 1900 La Plata, Argentina, Departamento de Química Física, Facultad de Química, Universidad de La Laguna, 38071 La Laguna, Tenerife, Spain, and Centro Atómico Bariloche, Comisión Nacional de Energía Atómica, 8400 S.C. de Bariloche, Argentina

Received: June 1, 2005; In Final Form: October 14, 2005

In this work, the electrochemical formation of alkanethiolate self-assembled monolayers (SAMs) on Ni(111) and polycrystalline Ni surfaces from alkanethiol-containing aqueous 1 M NaOH solutions was studied by combining Auger electron spectroscopy (AES), X-ray photoelectron spectroscopy (XPS), electrochemical techniques, and density functional theory (DFT) calculations. Results show that alkanethiolates adsorb on Ni concurrent with NiO electroreduction. The resulting surface coverage depends on the applied potential and hydrocarbon chain length. Electrochemical and XPS data reveal that alkanethiolate electroadsorption at room temperature takes place without S−C bond scission, in contrast to previous results from gas-phase adsorption. A complete and dense monolayer, which is stable even at very high cathodic potentials (−1.5 V vs SCE), is formed for dodecanethiol. DFT calculations show that the greater stability against electrodesorption found for alkanethiolate SAMs on Ni, with respect to SAMs on Au, is somewhat related to the larger alkanethiolate adsorption energy but is mainly due to the larger barrier to interfacial electron transfer present in alkanethiolate-covered Ni. A direct consequence of this work is the possibility of using electrochemical self-assembly as a straightforward route to build stable SAMs of long-chained alkanethiolates on Ni surfaces at room temperature.

1. Introduction

The preparation and characterization of alkanethiolate self-assembled monolayers (SAMs) on metals has attracted considerable attention because of the possibility of controlling order and interactions at the molecular level. This has triggered several innovative applications ranging from molecular electronics to biosensors. Most of the work has been done using Au, Ag, and Cu as substrates.[1−4] In contrast, the knowledge of the formation, physicochemical properties, and stability of SAMs on the highly reactive iron-group metals, particularly in aqueous solutions, is rather limited.[5] The implementation of straightforward methods for alkanethiolate film preparation on Ni surfaces would, in turn, facilitate their use in applications such as spintronics and electronics,[1−4] corrosion protection,[1−4] and as antiadherent layers in molds or stamps for pattern transfer in the micro- and nanoscale.[6,7]

In general, there are two main routes for SAM preparation: vapor-phase self-assembly (by and large performed in ultrahigh vacuum, UHV) and liquid-phase self-assembly.[8] UHV techniques are normally costly, and extended exposures are usually necessary to reach monolayer coverage. In contrast, liquid-phase self-assembly is the most popular method for SAM preparation because of its simple implementation, rapid attainment of monolayer coverage, and easy access to any laboratory.[1] For Au,[9−12] Ag,[13−15] and Cu,[16] it is done by simple immersion of the metal substrate in alkanethiol-containing ethanol, benzene, toluene, or hexane solutions and, in some cases, by immersion in pure liquid alkanethiols.

The presence of stable oxide layers normally hinders the reaction between the S headgroup of the organic molecule and the metal surface, thus resulting in poor-quality alkanethiolate SAMs.[5] The fact that alkanethiols actually self-assemble by liquid-phase preparation on Cu and Ag surfaces exposed to the atmosphere is because a redox reaction takes place between the metal oxide and the alkanethiol molecules. This reaction involves the oxidation of alkanethiols to sulfonates with the simultaneous reduction of silver[17] and copper[18] oxides to metallic Ag and Cu atoms, respectively. The fresh metallic layer easily reacts with the remaining alkanethiol molecules present in the solution to form the SAM. This appears not to be the case for iron-group metals, where the spontaneous reduction of the oxide is hindered.[19−21] Mekhalif et al. proposed a two-step procedure for alkanethiolate self-assembly on Ni involving as a first step the oxide electroreduction, followed by immediate substrate immersion in either pure alkanethiols or alkanethiol-containing ethanolic solutions.[19−21] However, in this procedure, the substrate is exposed to the atmosphere during the transfer process to the liquid, so that some amount of oxide is formed before the sample is immersed in the alkanethiol-containing solution. This has motivated us to search for alternative methods of alkanethiolate SAM formation on Ni.

On Au, electrochemical self-assembly from aqueous solutions containing alkanethiolate molecules has been successfully implemented.[22] There are no reports, to our knowledge, using this self-assembly method on Ni. However, NiO electroreduction

* To whom correspondence should be addressed. Tel.: 54-221-4257430. Fax: 54-221-4254642. E-mail: robsalva@inifta.unlp.edu.ar.
[†] Universidad Nacional de La Plata and CONICET.
[‡] Universidad de La Laguna.
[§] Comisión Nacional de Energía Atómica.

10.1021/jp052915b CCC: $30.25
Published on Web 11/19/2005

in aqueous solutions saturated with alkanethiol molecules may well be the most straightforward and direct route to form alkanethiolate SAMs on Ni because it can proceed in situ, it does not involve the use of organic solvents, and the electrochemistry of Ni in aqueous media is well understood. Basic physicochemical information needed to implement this procedure includes the following: (1) the nature and strength of the alkanethiolate−Ni bond, (2) the stability of the S−C bond under applied potential in aqueous environments, (3) the competition between H_2O, OH^-, and alkanethiolate molecules at different potentials, a crucial point for electrochemical self-assembly, and (4) the effect that the hydrocarbon chain length has on the electroadsorption and electrodesorption processes. While all of these issues are relevant, points 2 and 4 deserve particular attention for the following reasons. Point 2 is directly related to the integrity of the alkanethiolate SAM on the Ni surface. S−C bond scission has been observed in vapor-phase experiments on both Cu[23] and Ni,[24−27] depending on the initial substrate condition and alkanethiol coverage. For Cu, the formation of a S−methanethiolate surface mixture was observed with standing-wave method experiments.[23] On Ni, the onset of methanethiolate S−C bond scission was reported below room temperature for low methanethiol exposures[24−27] but above room temperature in the presence of preadsorbed S.[24] The onset temperature of S−C bond scission, on Ni, increases with coverage.[25] In contrast, for alkanethiolate films on Cu[28] and Ni[19−21] prepared in electrolyte solutions, the S−C bond remains intact at room temperature. Auger electron spectroscopy (AES) combined with electrochemical methods has revealed that alkanethiolate electrodesorption on Cu takes place in the hydrogen evolution reaction (HER) potential region, without S−C bond scission.[28] At present, however, no data have been reported on the state of the S−C bond for SAMs on Ni prepared in electrochemical environments. Point 4 refers directly to the SAMs' stability in aqueous electrolytes. While for SAMs on Au[29] and Ag[30] the stability potential range has been determined by recording the voltammetric peaks related to SAM electrodesorption, this procedure is not applicable to Ni. In fact, as in the case of SAMs on Cu,[28] no voltammetric evidence of electroadsorption/desorption can be observed because these processes occur in a potential range where the HER takes place at high rates. Thus, the faradaic current related to the HER completely masks any current related to possible SAM electrosorption.

In this study, we have addressed the four basic physicochemical aspects mentioned above by combining electrochemical methods, UHV surface analysis, and theoretical calculations based on density functional theory (DFT). Results obtained for propanethiol (C3), hexanethiol (C6), and dodecanethiol (C12) show that alkanethiolates adsorb on Ni surfaces as NiO electroreduction takes place. Alkanethiolate electroadsorption takes place without S−C bond scission, in contrast to previus results from gas-phase adsorption. The resulting surface coverage depends on the applied potential and hydrocarbon chain length. In the particular case of dodecanethiol, a complete and dense SAM that is stable even at very high cathodic potentials (−1.5 V vs SCE) is formed. DFT calculations show that the greater stability against electrodesorption found for alkanethiolate SAMs on Ni with respect to SAMs on Au, while related to the larger alkanethiolate adsorption energy, is mainly a consequence of the larger barrier to interfacial electron transfer present in alkanethiolate-covered Ni.

These results, besides providing insight into previously unaddressed physicochemical aspects of alkanethiolate self-assembly on Ni, suggest that electrochemical self-assembly from aqueous NaOH media saturated with alkanethiol is a straightforward route for building stable SAMs of long-chained alkanethiolates on Ni surfaces.

2. Experimental and Computational Procedures

2.1. Experimental Procedures. Alkanethiolate monolayers were self-assembled on button-shaped polycrystalline and Ni(111) electrodes and investigated both electrochemically and with ex situ AES and X-ray photoelectron spectroscopy (XPS). Ni buttons were machine and spark cut from grade 1 polycrystalline (Johnson Matthey Electronics) and Ni(111) (Goodfellows) rods, respectively. The electrodes were then polished with emery paper of different particle size, finished with 5-μm alumina paste, cleaned by alternating 5-min sonications first in high-purity water (purified using a Millipore Milli-Q system) and then in cyclohexane, followed by a final rinse in water, and finally dried under nitrogen. Ni(111) electrodes were further sputtered and annealed in UHV until a well-structured p(1 × 1) low-energy electron diffraction pattern was observed. In either case, after the final cleaning step, these Ni buttons were used as the working electrode in a conventional electrochemical cell.

The base electrolyte, a 1 M NaOH aqueous solution, was prepared with water previously purified using a Millipore Milli-Q system and solid NaOH (analytical grade from Baker) and was degassed with purified nitrogen for 2 h prior to the experiments. Three alkanethiols with different chain lengths n were used separately: propanethiol (C3), hexanethiol (C6), and dodecanethiol (C12). All of them were from Fluka and were used without further purification. Alkanethiols were introduced into the nitrogen-bubbled 1 M NaOH solution to obtain 5×10^{-3} M alkanethiol solutions. In the case of C6 and C12, the alkanethiol concentration exceeds the solubility limit in aqueous solutions,[31] resulting in saturated solutions.

A PAR model 362 potentiostat, which includes a function generator, and a conventional three-electrode glass cell, using a Pt large area wire as the counter electrode and a saturated calomel electrode (SCE) as the reference electrode, was used for the electrochemical measurements and for the electrochemical self-assembly.

Samples were prepared by introducing the Ni electrodes in the alkanethiol solution with an applied potential E_{ad} ranging from −0.5 to −1.6 V and, after 5 min, taking them out at the same E_{ad} value. Cyclic voltammograms between ca. −1.2 and −0.5 V, at sweep rates of 50 mV s^{-1}, were performed in the same electrolyte solutions. For ex situ spectroscopic and electrochemical measurements, the Ni electrodes were removed from the solution at E_{ad}, sonicated 5 min in absolute ethanol to minimize any possible readsorption from micelles present in the alkanethiolate-saturated 1 M NaOH solution, and immediately dried under a N_2 stream to minimize contamination.

The surface chemical composition of the alkanethiolate-covered Ni electrodes was analyzed by AES and XPS. The Auger spectra were measured with the electron gun operated at 3 keV and 10 mA cm^{-2}. Typically, two to four different samples and four or five points within a sample were investigated for each condition. The photoemission spectra were measured using the Al Kα line (1486.6 eV), with the X-ray gun operated at 240 W and an analyzer resolution of 1 eV. Typical acquisition times for survey, C 1s, and O 1s spectra were on the order of 10 min, while 2 h were necessary for S 2p spectra.

Further electrochemical checks were performed on Ni samples freshly prepared at specific E_{ad} values in the 5×10^{-3} M

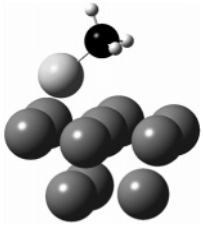

Figure 1. $Ni_{10}-SCH_3$ cluster used for DFT calculations. Ni atoms are in gray, S in light gray, C in black, and H in white.

alkanethiolate solutions, by subsequently wetting the Ni electrodes in 0.1 M HCl (prepared from Merck analytical grade reagent, 37%) solutions with the meniscus method[32] and etching the Ni electrode from −0.75 V positive, at a sweep rate of 10 mV s^{-1}, until near the onset of Ni electrodissolution.

S blanks were prepared from 10^{-3} M Na_2S (Alfa Aesar) in 1 M NaOH aqueous solutions and investigated following similar electrochemical and spectroscopic procedures.

Comparisons were also established with Au working electrodes. In particular, electrodesorption potentials for SAMs of C3, C6, and C12 on Au were measured from voltammetric runs made at 50 mV s^{-1}, following the procedure described in refs 28 and 30. Briefly, Au thin films prepared by evaporation on glass (AF 45 Berliner Glas KG, Berlin, Germany) were used as substrates. After annealing for 3 min with a hydrogen flame, these Au substrates exhibited atomically smooth (111) terraces separated by monatomically high steps. The Au electrodes were then used as working electrodes in the electrochemical cell containing 5×10^{-3} M alkanethiol + 1 M NaOH aqueous solutions to estimate electrodesorption potentials.

2.2. DFT Calculations. The adsorption energies of a negatively charged methanethiolate anion (CH_3S^-) on Ni(111) surface sites were estimated by using DFT, following recently reported procedures for Au(111), Ag(111), and Cu(111) surfaces.[28,30] As for Au, Ag, and Cu, we consider the adsorption energy of the negatively charged organic species because the reductive electrodesorption process in aqueous media results in alkanethiolate anion formation.

DFT calculations are based in the three-parameter hybrid method proposed by Becke, associated with the gradient-corrected correlation functional of Lee, Yang, and Parr, B3LYP.[33] The Ni atoms have been described with 10 electrons, whereas the remainder of the atomic electron density was replaced by a relativistic effective core potential (ECP) from Hay and Wadt, LANL1MB.[34] The valence shell was treated explicitly with the basis set LANL1MB. S, C, and H atoms are described with the standard 6-31G(d) basis set,[35] which is of split valence plus polarization quality. In all cases, the electronic state considered is taken as the lowest energy closed-shell configuration. Despite the fact that Ni surfaces are magnetic, we have not taken into account the spin polarization effects in these calculations given that magnetization does not alter the adsorption structures.[36] The theoretical calculations were performed with the electronic structure software *Gaussian98*.[37] We have also calculated the charge remaining in the S atom after methanethiolate adsorption by using Mulliken populations. These are used as a qualitative tool because of their well-known limitations.

The cluster model used to represent the metal surface was built with 10 atoms, distributed 7 in the top layer and 3 in the second layer (Figure 1). The Ni−Ni distance was maintained fixed to the bulk value of 0.249 nm.[38] We have explored four surface sites: hollow hexagonal close packed (hcp), hollow face-centered cubic (fcc), bridge, and top. The methanethiolate anion

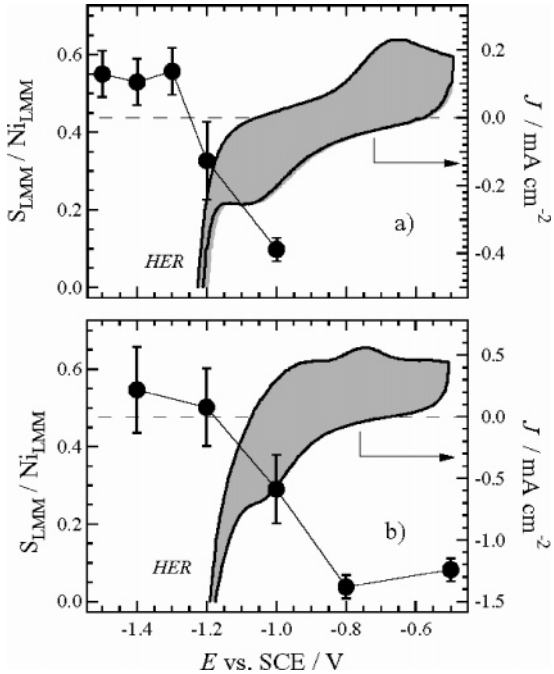

Figure 2. S_{LMM}-to-Ni_{LMM} AES signal ratios (left) recorded for Ni(111) (a) and Ni_{poly} (b) electrodes polarized in a C12 solution (5 mM C12 in 1 M NaOH) for 5 min at different potentials E_{ad}, superimposed on polarization curves (right) taken at 50 mV s^{-1}, for the same electrode−electrolyte systems.

was oriented with the S atom pointing toward the metal surface at a certain distance over the selected surface site. The S−Ni distance (d) and the angle α defined between the C−S bond and the substrate normal were optimized, while holding the rest of the anion geometry fixed, throughout the calculations, at the optimized values of the isolated anion.

The methanethiolate adsorption energy, E_{ads}, has been defined as

$$E_{ads} = E[Ni_{10}SCH_3^-] - \{E[Ni_{10}] + E[SCH_3^-]\} \quad (1)$$

where $E[Ni_{10}SCH_3^-]$ is the total energy of $Ni_{10}SCH_3^-$ with the parameters d and α optimized, $E[Ni_{10}]$ is the energy for the metal cluster, and $E[SCH_3^-]$ is the energy of the methanethiolate anion.

3. Experimental Results

3.1. Electrochemical Self-Assembly of Dodecanethiolate on Ni(111). A typical voltammogram for a Ni(111) electrode recorded from −0.5 to −1.4 V in a saturated C12 (5 mM) 1 M NaOH solution at v = 50 mV s^{-1} is shown in Figure 2a (continuous curve, right axis). The Ni(111) electrode exhibits a cathodic peak at ca. −1.05 V, related to the electroreduction of NiO,[39] preceding the large cathodic current related to the HER. The positive scan shows the peak corresponding to the electroformation of NiO, located at −0.70 V. As in the case of alkanethiol electrosorption on Cu electrodes,[28] there are no distinct current peaks associated with dodecanethiol electrosorption on the Ni electrode. Assuming that, as in the case of Cu, alkanethiol electrosorption could take place in the HER potential region, complementary methods must be utilized to investigate these processes.

Figure 3a shows the AES spectra of a sputter-cleaned Ni(111) surface and of two Ni(111) electrodes after polarization in the saturated dodecanethiol-containing solution at E_{ad} = −1.0 and −1.3 V, i.e., right at the onset and at the end of the NiO

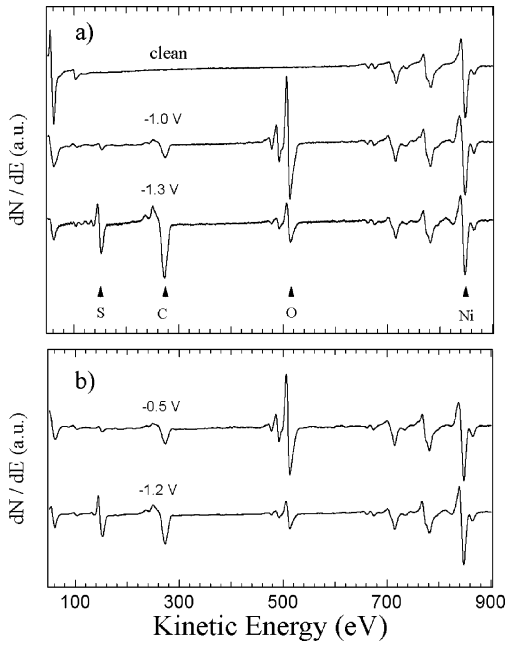

Figure 3. AES spectra for Ni(111) (a) and Ni_{poly} (b) electrodes polarized in a C12 solution for 5 min at the E_{ad} values indicated. The arrows at the bottom of panel (a) identify the peaks corresponding to the S_{LMM}, C_{KLL}, O_{KLL}, and Ni_{LMM} Auger transitions. A spectrum of Ni(111) cleaned in UHV is included.

electroreduction peak in the voltammogram. The peaks in the AES spectrum of the clean Ni(111) surface at 61 eV and in the region around 750 eV correspond to the MNN and LMM transitions of Ni, respectively.[40] The spectrum of the sample polarized at $E_{ad} = -1.0$ V presents a large O_{KLL} peak (510 eV) and two smaller peaks due to C_{KLL} (272 eV) and S_{LMM} (152 eV).[40] The oxygen peak clearly indicates that there is still an important oxide layer on the surface; some adsorption, however, has already taken place, as evidenced by the S peak; the C peak is ascribed partly to the adsorbed thiols and partly to atmospheric contamination during transport of the sample in air to the UHV chamber. In the spectrum of the sample polarized at $E_{ad} = -1.3$ V, there are important changes of the S, C, and O signals: the first two increase notably, while the O signal decreases dramatically. These changes strongly suggest that electroadsorption of S- and C-containing species is associated with the electroreduction of NiO.

Returning to Figure 2a, data points correspond to peak-to-peak S_{LMM} signals, normalized by the main Ni_{LMM} (~848 eV) signal (left axis), recorded for Ni(111) polarized in dodecanethiol-containing solutions at different potential values -1.5 V $< E_{ad} < -1.0$ V (bottom axis), superimposed on the Ni(111) voltammogram recorded in the same electrolyte. Each data point corresponds to an average S_{LMM} value obtained by sampling different points on several samples prepared at that particular E_{ad}. Error bars indicate the standard deviation of the measurements; the standard deviation is larger than any systematic experimental uncertainty.

On average, the S_{LMM}-to-Ni_{LMM} ratio starts to increase for $E_{ad} < -1.0$ V, when the NiO electroreduction peak in the voltammogram begins to grow, and approaches a plateau at $E_{ad} = -1.3$ V, just after the completion of the NiO electroreduction peak. This indicates that dodecanethiol adsorption is allowed (at appreciable rates) because the electroreduction of NiO leaves free Ni sites on the electrode surface.

The thiol coverage, defined as the number of adsorbed thiol molecules per surface Ni atom, was estimated in the following way:

$$\theta = \frac{I_S}{I_{Ni}[1 - e^{-1/\lambda}]} s_{Ni}^{S} e^{nd \cos\phi(1/\lambda_{152} - 1/\lambda_{778})} \quad (2)$$

where I_S is the S_{LMM} (152 eV) peak-to-peak signal height, I_{Ni} is the Ni_{LMM} (778 eV) peak-to-peak signal height, s_{Ni}^{S} is the Ni_{LMM} sensitivity relative to S_{LMM}, evaluated from standard spectra,[40] λ (in monolayers) is the effective attenuation length in Ni of 778-eV electrons,[41] nd is the extended chain length in an all-trans geometry, ϕ is the tilt angle, and λ_{152} and λ_{778} are the attenuation lengths in the thiol layer of 152- and 778-eV electrons, respectively.[42] The factor in brackets is to take into account the fact that the Ni signal comes from a semi-infinite Ni layer, and we are interested only in the outermost layer. By replacing the average 0.55 value reached by the S_{LMM}-to-Ni_{LMM} ratio (Figure 2) into eq 2, one obtains $\theta \approx 0.37$; i.e., a monolayer of adsorbed dodecanethiol on Ni has been formed.

Correlated with the rise of the S_{LMM} signal in passing across the NiO electroreduction peak, one would expect to see a similar rise of the C_{KLL} signal as well as a fall of the O_{KLL} signal. While the average trend followed by these signals responds to this behavior, experimental scatter is much larger than that for S_{LMM}, most probably because of atmospheric contamination during the sample transfer in air from the electrochemical cell to the AES chamber.

It is clear from Figure 2a that the maximum coverage is obtained well within the HER region. This explains why no peaks associated with alkanethiol electroadsorption/electrodesorption are observed in the cyclic voltammograms. The absence of this pair of peaks precludes the possibility of determining the total charge transferred during the electroadsorption reaction. This would serve as another measure of the final surface coverage associated with the adsorption of the dodecanethiol molecule.

The next issue to address is the identity of the species that are adsorbed on the Ni surfaces. It is known that S−C bond scission occurs for methanethiol[24,26,27] and dimethyl disulfide[25] adsorbed from the vapor phase on Ni(111). At about 150 K, there is just one species, namely, the chemisorbed methanethiolate molecules, but when the methanethiolate−Ni surface is annealed at temperatures slightly below room temperature, another species appears, identified as atomic S. The S−C bond scission producing this new species is particularly important because atomic S, instead of protecting the Ni surface, enhances electrodissolution.[43] To determine whether S−C bond cleavage occurs, we have measured XPS spectra in the region of the S 2p peak. Figure 4a presents the spectrum corresponding to Ni(111) polarized in a dodecanethiol-containing solution at $E_{ad} = -1.4$ V. The S 2p peak is asymmetric, with a tail toward higher binding energies. Two components were needed to fit this spectrum; each component was composed of two Voigt peaks separated by 1.18 eV and with a branching ratio of 0.5 representing the spin−orbit split S $2p_{3/2}$ and $2p_{1/2}$ levels;[44] the Gaussian and Lorentzian widths were 2.0 and 0.1 eV, respectively, for all of the Voigt peaks. Both a linear and a Shirley background were tested, yielding similar results. Fitting with two S 2p components, one obtains the main component at 162.6 eV ($2p_{3/2}$) and the minor component at 165.0 eV. These binding energies must be compared with those listed in Table 1 corresponding to S and alkanethiol adsorption on Ni. It can be seen in this table that chemisorbed S, chemisorbed molecules, and physisorbed species broadly fall between 161 and 162 eV, between 162 and 163 eV, and between 163 and 164 eV,

TABLE 1: S $2p_{3/2}$ Binding Energies (BEs) of Selected Sulfur and Sulfur-Containing Molecules on Ni, with R = $(CH_2)_nCH_3$ Except Where Noted

	S species	BE (eV)	system	ref
sulfur	sulfide	161.00	NiS	46
	chemisorbed	161.15−162.10	Ni(100) and Ni(111)	25 and 26
	bulk	163−164	S^0, S_n, multilayers	44
alkanethiol RS^- or RSH	chemisorbed	161.8	Ni_{poly}	19−21
		162.00−163.35	Ni(100) and Ni(111)	25 and 26
		162.5	$HS(CH_2)_{10}COOH$ on Ni(111)	48
	physisorbed	163.3	Ni_{poly}	19
dialkyl disulfide RSSR	physisorbed	164.35	Ni(111)	25

respectively. Therefore, we can make a preliminary assignment of our main component at 162.6 eV to chemisorbed dodecanethiolate. The small component at 165.0 eV falls, just above these ranges. It is, notwithstanding, very close to the 164.35 eV reported for dimethyl disulfide on Ni,[25] hinting to the possible formation of a thiol−thiol bond. It is even closer to the 164.9 eV value reported for alkanethiol micelles on Pd.[45] The minor component can therefore be associated with a thiol−thiol interaction, very probably due to the formation of micelles.

We have also fitted the spectra with three components, finding only a negligibly small component at binding energies smaller than 162.6 eV. The absence of any noteworthy component below 162 eV would discount the existence of any significant amount of atomic S in the form of nickel sulfide.[46] Nevertheless, the presence of submonolayer S amounts cannot be entirely ruled out because, for NiS_2 compounds[47] and Na_2S adsorption on Pd(111),[45] S $2p_{3/2}$ binding energies of 162.7 and 162.8 eV have been measured, respectively.

Further evidence in favor of the integrity of the molecules is provided by electrochemical polarization curves. Figure 5a shows polarization curves for dodecanethiolate-covered Ni(111) electrodes performed in acidic (aqueous 0.1 M HCl) electrolytes, compared with polarization curves of clean and S-covered Ni(111) electrodes. S and C12 surfaces were prepared by initially polarizing Ni(111) for 1 min at $E_{ad} = -1.3$ V in Na_2S- and C12-containing NaOH solutions, respectively. "Clean" Ni electrodes were obtained by polishing Ni surfaces with a 5 μm alumina grit just prior to polarization. The HER was used to test the cleavage of the alkanethiolate species on the Ni surface.

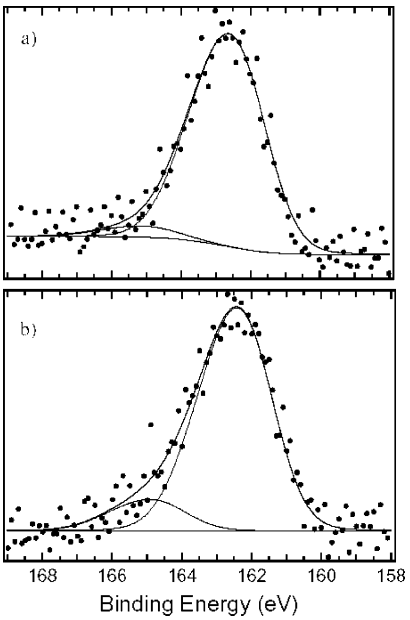

Figure 4. S 2p photoelectron spectra of Ni(111) (a) and polycrystalline Ni (b) polarized for 5 min in C12 solutions at $E_{ad} = -1.4$ and -1.2 V, respectively. Dots represent data points, and curves, the results of the best fit.

The HER proceeds through the following reaction:

$$e^- + H_2O = OH^- + \frac{1}{2}H_2 \qquad (3)$$

Charge transfer through the long hydrocarbon chains is normally difficult[49] so that for C12 the HER reaction should take place mainly at SAM defects and, accordingly, it should be hindered in relation to clean or S-covered Ni. In fact, for Ni−S electrodes, a smaller overpotential for the HER with respect to clean Ni has been reported.[50] Results for the dodecanethiolate-covered Ni(111) surfaces show that the HER involves an overpotential of about 0.2 V with respect to uncovered (i.e., clean) and S-covered Ni(111), while no striking differences are observed between Ni(111) and S-covered Ni(111). From these results, one can conclude that in aqueous electrolytes no significant cleavage of the S−C bond takes place. These results parallel those reported for alkanethiolate adsorption on Cu(111) surfaces from aqueous solutions, where alkanethiolate electrodesorption takes place without S−C bond scission.[28] Note that on both Cu(111)[23] and Ni(111)[24−27] the onset of S−C bond scission occurs at or below room temperature for vapor-deposited alkanethiol films.

In summary, we have shown that dodecanethiol molecules can be electroadsorbed on Ni(111) electrodes in the HER region, can reach a surface coverage close to that of a complete monolayer, and can form thiolate bonds. Returning to our quest to try to find a simple way of assembling alkanethiol molecules on Ni, the next query then is whether these results hold true for

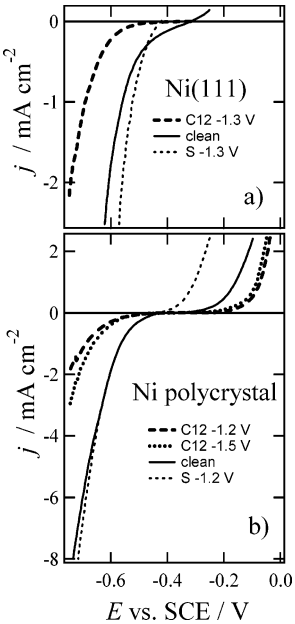

Figure 5. Polarization curves for dodecanethiol-covered, S-covered, and clean Ni samples, as indicated, taken in 0.1 M HCl at 50 mV s^{-1} from −0.75 V until near the onset of Ni electrodissolution, for both Ni(111) (a) and polycrystalline Ni (b).

a generic Ni electrode. In the following subsection, we repeat, with polycrystalline electrodes, the experiments performed on Ni(111) electrodes.

3.2. Electrochemical Self-Assembly of Dodecanethiolate on Polycrystalline Ni. Figure 2b shows a typical voltammogram recorded for polycrystalline Ni (Ni_{poly}) in the dodecanethiol-saturated 0.1 M NaOH aqueous solution. A cathodic peak at ca. −1.0 V, related to the electroreduction of NiO, is observed preceding the HER, while electroformation of NiO takes place at −0.75 V. As a result of more crystallographic planes being exposed to the electrolyte, the voltammogram for NiO electroreduction/electroformation shows broader features than those observed for Ni(111). Again, no evidence of dodecanethiol electroadsorption/electrodesorption was detected in the voltammetric runs. However, dodecanethiol does adsorb on the surface, as revealed by the AES spectra (Figure 3b). It is seen again that the S and C signals increase only after the O signal decreases, implying again that alkanethiol electroadsorption proceeds as NiO electroreduction leaves clean Ni sites. The S_{LMM}-to-Ni_{LMM} AES ratio for the polycrystalline surface is shown in Figure 2b. In this case, the increase from around 0.1 to 0.6 occurs over a broader applied potential range, as a result of the electroreduction of NiO occurring at slightly different potentials for each crystallographic surface plane and therefore leaving free Ni sites at slightly different potentials on each Ni_{poly} grain. The C uptake follows the S uptake but with a more erratic behavior caused by the atmospheric contamination during the sample transfer to the UHV chamber; something similar occurs with the decrease of the O signal. The broader potential range for NiO electroreduction and probable larger reactivity of certain Ni crystallographic orientations in Ni_{poly} results in monolayer C12 coverages at $E_{ad} = -1.2$ V, i.e., nearly 0.1 V more positive than that on Ni(111).

Figure 4b shows the S 2p XPS spectrum of C12 polarized for 5 min at $E_{ad} = -1.2$ V, as indicated. For C12 electroadsorbed on Ni_{poly}, the S 2p signals again show the two components described for C12 on the Ni(111) substrate, with the main component at 162.4 eV and the small second component at 164.8 eV. Once again we associate the main component with a thiolate species. Notice that this assignment has been strongly supported by the conclusions reached for the Ni(111) substrate. On the other hand, our experimental data do not allow us to make a firm assignment of the small component. Once again, we tentatively assign it to alkanethiol micelles or other clustering due to thiol−thiol interactions.

To test the possible cleavage of the alkanethiolate molecules on the Ni_{poly} surface, we have recorded polarization curves (Figure 5b) akin to those shown in Figure 5a for Ni(111) but including also the anodic branch of the polarization curves, where Ni electrodissolution takes place.

The cathodic branch of the polarization curves shows trends similar to those seen on Ni(111): the dodecanethiolate-covered Ni_{poly} strongly hinders the HER, while S is not able to produce this effect. As for Ni(111), one can conclude that no significant cleavage of the S−C bond takes place in the potential range between the electroreduction of NiO and the onset of the HER.

In the anodic branch of the polarization curves, Ni electrodissolution proceeds according to the following reaction:

$$Ni = Ni^{2+} + 2e^- \quad (4)$$

Figure 5b shows that, with respect to clean Ni, S strongly enhances the electrodissolution process, whereas dodecanethiolate SAMs strongly inhibit this process, confirming both the integrity of the molecule and the increased electrode protection against corrosion. Note that we have not performed a similar study on the electrodissolution of Ni(111) in order to avoid irreversible damage to the single-crystal surface by development of etch pits.

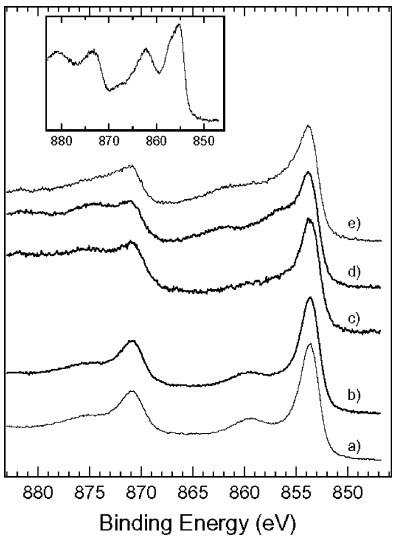

Figure 6. Ni 2p XPS spectra of Ni_{poly} polarized for 5 min in C12 solutions at $E_{ad} = -1.2$ V (b), −1.6 V (c), and −0.5 V (d), respectively. Ni_{poly} electrodes cleaned (a) and exposed to 1000 L of O_2 (e), in UHV, are also shown. The inset corresponds to NiO.

We now focus our attention on the minor differences between overpotentials for C12 electroadsorbed at $E_{ad} = -1.2$ V with respect to C12 electroadsorbed at $E_{ad} = -1.5$ V, in both the HER and the Ni electrodissolution regions. One could speculate that this small difference in potential (smaller overpotential for both reactions in the sample polarized at $E_{ad} = -1.5$ V) is due to the onset of dodecanethiolate electrodesorption as E_{ad} moves negatively, such as occurs for alkanethiolates adsorbed on Au(111), Ag(111), and Cu(111) surfaces.[9−15,28−30] Alternatively, this decrease in the overpotential protection could also be associated with the onset of S−C bond scission.

Additional information about the dodecanethiolate-covered polycrystalline surfaces is provided by the Ni 2p XPS spectra shown in Figure 6, corresponding to C12 electroadsorbed on electrodes polarized at $E_{ad} = -0.5$, −1.2, and −1.6 V. Also included for comparison are the spectra of a clean metal surface and one of a Ni surface exposed to 1000 L of O_2 in UHV. The oxidation of Ni in UHV produces a gradual shift of the Ni $2p_{3/2}$ and $2p_{1/2}$ peaks toward higher binding energies and the disappearance of the characteristic satellite at 860 eV,[44] which is gradually replaced by other structures; the spectrum eventually reaches the form of the NiO spectrum shown in the inset. It is seen in Figure 6 that the best dodecanethiolate layer is obtained when the electrode is immersed in the C12 solution at $E_{ad} = -1.2$ V. At this potential, the Ni 2p spectrum perfectly resembles that of the clean Ni surface, while at $E_{ad} = -0.5$ and −1.6 V, the Ni 2p spectra look more like the spectrum of the slightly oxidized surface. This has a 2-fold implication. First, at $E_{ad} = -1.2$ V, the native oxide on the surface was totally removed and replaced by the C12 SAM, and second, the SAM, in turn, was quite effective in protecting the electrode against oxidation during transport to the UHV chamber. Films of similar quality, as determined from the Ni 2p spectra, were obtained by Mekhalif et al.[21] after 18 h of immersion in pure C12, at open-circuit potential, following a two-step procedure.

In summary, dodecanethiolate can be chemisorbed on polycrystalline Ni. The best films are obtained for electrodes polarized at $E_{ad} = -1.2$ V. The electrochemical measurements

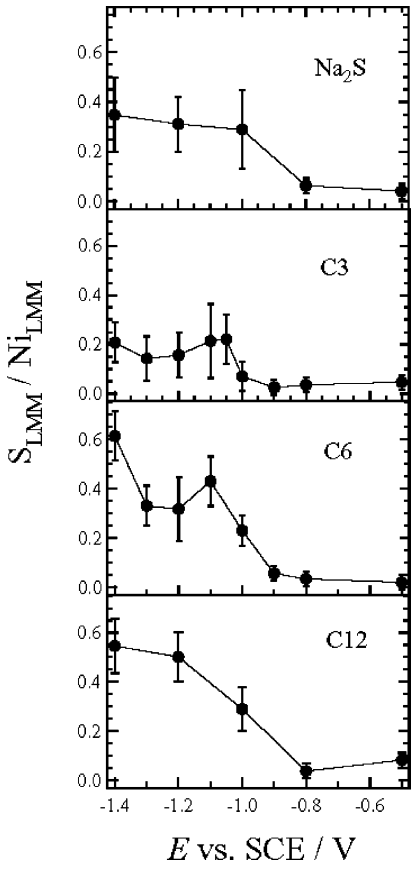

Figure 7. Average S_{LMM}-to-Ni_{LMM} AES signal ratios of Ni_{poly} electrodes polarized in Na_2S, C3, C6, and C12 solutions for 5 min at different E_{ad} values.

show that dodecanethiolate molecules remain intact, similar to what was observed for Ni(111) surfaces.

In the next section, we explore the role of van der Waals interactions and hydrophobic forces in alkanethiolate electroadsorption on Ni.

3.3. Electrochemical Self-Assembly of Alkanethiolates on Ni Surfaces: Chain-Length Effects. To gain further insight into the effects of van der Waals interactions and hydrophobic forces on the electrochemically induced self-assembly of alkanethiols on Ni, C3 and C6 were also electroadsorbed on Ni_{poly} following the same procedure as that described for C12. AES S_{LMM}-to-Ni_{LMM} ratio signals were used to monitor the alkanethiol electroadsorption at different E_{ad} values covering a broad potential range.

The information derived from the AES spectra is summarized in Figure 7. Each S_{LMM} signal is the result of averaging all measured S_{LMM} signals at each E_{ad} for solutions containing sodium sulfide, C3, C6, and C12. Error bars indicate the standard deviation of the measurements; the standard deviation is larger than any systematic experimental uncertainty.

The first feature to take note of in Figure 7 is the S-signal increase for $E_{ad} < -0.9$ V in all four panels, just at the beginning of NiO electroreduction. This fact, by analogy with the C12 case, shows that S, C3, and C6 also adsorb because the NiO electroreduction leaves free Ni sites. However, we note several differences with respect to the electroadsorption of C12. The first is that the final coverage at the completion of NiO electroreduction is smaller for S, C3, and C6 than for C12. The others are related to the behavior of the S_{LMM}-to-Ni_{LMM} signal ratios in the range between -0.8 and -1.4 V. While for S and C12 this signal increase is monotonic, for C3 and C6 it is more complex, with both presenting local maxima near -1.1 and -1.4 V.

We first focus on the S coverage attained near the completion of the electroreduction of NiO. As was already stated, the S_{LMM}-to-Ni_{LMM} signal ratio of C12 is close to the 0.6 value expected for a complete monolayer ($\theta \sim 0.33$). The somewhat smaller values of 0.45 ($\theta \sim 0.25$), 0.2 ($\theta \sim 0.11$), and 0.3 ($\theta \sim 0.17$) measured for C6, C3, and S, respectively, indicate that the self-assembly process for the shorter-chain alkanethiols and S is not as effective at reaching a complete monolayer. The surface coverage by the alkanethiolate species decreases despite the fact that their concentration, given by the alkanethiolate solubility in aqueous solution, is larger for C3 than for C12.[31] Increasing the adsorption time from 5 to 100 min has resulted in no significant changes in the S signals, suggesting that van der Waals interactions and hydrophobic forces are not the only factors governing the kinetics of alkanethiol self-assembly on Ni. In the case of S, the approximate maximum coverage of $\theta = 0.2$ is close to that expected for a p(2 × 2) structure.[52]

We next focus on the S_{LMM}-to-Ni_{LMM} maxima observed for C3 and C6 at $E_{ad} = -1.05$ and -1.1 V, respectively. One possible origin of the local maxima could be the onset of alkanethiolate electrodesorption, resulting in a decrease in the S signals at E_{ad} values more negative than these. In this case, alkanethiolate electrodesorption would shift in the negative direction with increasing chain length. The stability of C12 against electrodesorption will be discussed in more detail in the following sections. However, it can be said that, for the longer-chain alkanethiols, van der Waals interactions and hydrophobic forces play an important role, first by promoting alkanethiolate self-assembly and second by stabilizing the assembled layer with increasing chain length. The lack of evidence for S desorption is consistent with the adsorption energy of the double negatively charged S^{2-} on Ni being higher than that of alkanethiolates.[53]

For all three alkanethiols investigated, there is an apparent increase in the S coverage going from $E_{ad} = -1.3$ to -1.4 V, as well as a larger scatter in the *S* values. The coverage increase is particularly evident for hexanethiol, which at $E_{ad} = -1.4$ V reaches an S_{LMM}-to-Ni_{LMM} intensity ratio similar to that of C12. Different processes could be responsible for such behavior. One possibility is that the bubbling produced during the HER facilitates micelle physisorption from the saturated alkanethiolate solutions[31] onto the Ni sites left free by alkanethiolate electrodesorption. This is based on the fact that, even for unsaturated solutions, evidence of micelle formation following C6 electrodesorption has been observed on Au.[54] Another possibility is that, because of the much higher hydrogen concentration (pressure) in the solution, hydrogen could penetrate easier in regions left free by desorbed alkanethiolates, especially for shorter-chain alkanethiols, promoting S−C bond scission and then leading to chemisorbed S and the corresponding hydrocarbon. The later is based on the observation that hydrogen promotes S−C bond scission.[24] With our current data, we cannot determine which processes are involved in the S signal increase for $E_{ad} < -1.3$ V. Further work is needed in this direction.

Obviously, atmospheric C and O contamination for the shorter chains and at very negative potentials is also more important, as a result of less Ni being protected by the alkanethiolate species during the transfer procedure to the UHV chamber. This results in very erratic O_{KLL} and C_{KLL} signals. Therefore, while for C12 some trends could be followed from O_{KLL} and C_{KLL} signals, this is practically impossible for C3 and C6. In

particular, C contamination prevents any reliable correlation between the S and C signals.

In summary, results obtained for S, C3, C6, and C12 indicate that alkanethiolates adsorb in aqueous alkaline solutions concurrently with NiO electroreduction, irrespective of the hydrocarbon chain length. The surface coverage at the completion of NiO electroreduction is, however, largely influenced by the hydrocarbon chain length, increasing in the following order: C3 < C6 < C12. Electrochemical self-assembly to form complete alkanethiolate monolayers should be possible for C ≥ 12.

The stability region of these alkanethiolates on Ni against electrodesorption has not yet been established and will be discussed in the following sections.

4. Discussion

4.1. Electrochemical Reactions. Contrary to what is observed for Ag_2O[17] and CuO,[18] the reduction of NiO with simultaneous oxidation of the alkanethiol to sulfonates and self-assembly of alkanethiol at oxide-free sites do not occur at an appreciable rate in the aqueous alkaline solutions. In fact, the S signal only increases significantly in the electroreduction potential region of NiO.

It is generally accepted that in nonaqueous solvents the self-assembly reaction on metals proceeds by the reaction 5a.

$$(CH_3)(CH_2)_nSH + M = (CH_3)(CH_2)_nS{-}M + \frac{1}{2}H_2 \quad (5a)$$

However, the pK of propanethiolate in water is p$K \cong 9$[55] so that at pH 14 most of the alkanethiol molecules exist as alkanethiolate anions. Therefore, the main reaction involved in alkanethiolate self-assembly from aqueous 1 M NaOH should be

$$(CH_3)(CH_2)_nS^- + M = (CH_3)(CH_2)_nS{-}M + e^- \quad (5b)$$

rather than reaction 5a. The complete electrochemical self-assembly process on Ni can thus be described by the following reactions:

$$2e^- + NiO + H_2O = Ni^* + 2OH^- \quad (6a)$$

$$(CH_3)(CH_2)_nS^- + Ni^* = (CH_3)(CH_2)_nS{-}Ni + e^- \quad (6b)$$

where the asterisk denotes a Ni site produced by the NiO electroreduction reaction. From eq 6a, it becomes clear that the self-assembly process is dominated by the rate of NiO electroreduction. While reaction 6a explains the main dependence of the S signal (the fingerprint of the thiol molecule) with E_{ad}, the surface coverage dependence on the hydrocarbon chain length can be explained considering van der Waals interactions and hydrophobic forces acting at SAMs. In fact, as the number of C atoms increases, these stabilizing forces increase, leading to a surface coverage compatible with a complete and dense monolayer. These observations agree with the behavior of C3 and C12 SAMs on Au. In fact, C3 SAMs exhibit missing rows and a large number of molecular defects[56] even for adsorption times as long as 24 h in ethanolic solutions. Conversely, for longer-chain alkanethiols, such as dodecanethiol, times on the order of minutes are sufficient to attain coverages compatible with a complete monolayer.

On Au,[9−12,29,30] Ag,[13−15,30] and Cu,[28] alkanethiolate electrodesorption takes place at specific potential values that depend on both the alkanethiol chain length and the nature of the substrate. We have recently proposed[28,30] that the reductive desorption process of an alkanethiolate molecule from a metal substrate in a solvent (solv) can be described by the following reaction steps, which in the case of Ni can be written as

$$(CH_3)(CH_2)_nS{-}Ni + e^- = [(CH_3)(CH_2)_nS{-}Ni^-] \quad (7)$$

$$[(CH_3)(CH_2)_nS{-}Ni^-] = (CH_3)(CH_2)_nS^- + Ni \quad (8)$$

$$(CH_3)(CH_2)_nS^- + \text{solvent} = [(CH_3)(CH_2)_nS^-]_{solv} \quad (9)$$

$$Ni + \text{solvent} = Ni_{solv} \quad (10)$$

where Ni_{solv} stands for a Ni atom with an adsorbed solvent molecule. The energy barrier to desorb an alkanethiolate molecule from the Ni surface should involve alkanethiolate−Ni (E_{A-S}), alkanethiolate−alkanethiolate (E_{A-A}), alkanethiolate−solvent (E_{A-s}), and Ni−solvent (E_{S-s}) interaction energies. The energy involved in eq 7 (E_{ct}) is related to the energy needed to introduce an electron into the alkanethiolate−metal system, i.e., the energy related to the charge-transfer process. Equation 8 involves the n-independent desorption energy $E_{des} = -E_{ads}$.[28,30] Therefore, E_{A-S} contains both E_{ct} and E_{des}. Equation 9 involves the breaking of hydrocarbon chain−hydrocarbon chain interactions (E_{A-A}) and E_{A-s}. Finally, eq 10 involves E_{S-s}.

The energy (E_{ed}) involved in the electrodesorption process can be written as

$$E_{ed} = E_{des} + E_{A-s} + E_{A-A} + E_{S-s} + E_{ct} \quad (11)$$

For $n = 0$, the n-dependent terms E_{A-s} and E_{A-A} cancel so that eq 11 becomes

$$E_{ed}^{n=0} = E_{ct} + E_{des} + E_{S-s} \quad (12)$$

The value for water adsorption on Ni is $E_{S-s} = -69$ kJ mol^{-1} from thermodynamic data[57]and 50 kJ mol^{-1} from DFT calculations[58] and is higher than that reported for water adsorption on Au ($E_{S-s} = -25.78$ kJ mol^{-1}).[59] Work function measurements provide good values for E_{ct}; however, very little data are available for alkanethiolate−metal systems. The energy (ϵ_{HOMO}) of the highest occupied molecular orbital (HOMO) is a measure of the alkanethiolate−metal cluster's ability to donate/accept electrons. It provides a good estimate for E_{ct} given that ϵ_{HOMO} can be considered a true ionization potential.[60] Therefore, we used the position of the ϵ_{HOMO} of the negatively charged alkanethiolate−Ni cluster to estimate the energy involved in the reverse of reaction 7.

4.2. DFT Calculations: Numerical Results and Electrochemical Stability of Alkanethiolates on Ni(111). Results obtained for the methanethiolate anion adsorption on Ni(111) surfaces are summarized in Table 2 and compared to those previously reported for methanethiolate adsorption on Au(111).[28] S−Ni bond lengths (d) are smaller and E_{ads} values are greater than those calculated for methanethiol adsorption on Au(111) surfaces.[28] The most favorable adsorption sites are hollow fcc, followed by the hollow hcp and bridge sites. These same trends are also followed by the neutral thiol species.[61] Finally, ϵ_{HOMO} is lower and the charge remaining on the S atoms is of the same magnitude as that estimated for Au(111) surfaces.

Before introduction of these values in the expression for E_{ed}, it is important to mention that combined NIXSW (normal incidence X-ray standing wave) and NEXAFS (near-edge X-ray absorption fine structure) results suggest equal occupations of hollow fcc and hollow hcp sites for methanethiolate molecules

TABLE 2: Optimized Parameters from DFT Calculations

metal cluster	site	d (nm)	α (deg)	$-E_{ads}$ (kJ mol^{-1})	ϵ_{HOMO} (eV)	charge on the S atom
$Au_{10}(111)$[a]	hcp	0.227	23.8	246	−1.18	−0.13
	fcc	0.232	58.5	255	−1.08	−0.15
	top	0.260	73.5	209	−1.23	−0.21
	bridge hcp	0.233	50.5	250	−1.19	−0.16
	bridge fcc	0.236	30.0	249	−1.22	−0.18
	bridge	0.234	24.9	226	−1.20	−0.18
$Ni_{10}(111)$	hcp	0.190	46.8	279	−0.70	−0.16
	fcc	0.184	47.8	286	−0.82	−0.10
	top	0.229	63.1	233	−0.82	−0.27
	bridge	0.198	53.9	272	−0.80	−0.18

[a] Data for Au were taken from ref 28.

on Ni(111).[27] On the basis of these observations, we have used $E_{des} = (1/2)(E_{des\ hcp} + E_{des\ fcc})$ and $\epsilon_{HOMO} = (1/2)(\epsilon_{HOMO\ hcp} + \epsilon_{HOMO\ fcc})$ for Ni(111), while for Au(111), we have indistinctly used bridge hcp and bridge fcc values.[28] By introducing these average ϵ_{HOMO} and E_{des} values (Table 2) and E_{S-s},[57,58] we obtain

$$E_{ed}^{n=0}[\mathrm{Ni(111)}] = -73.06\ \mathrm{kJ\ mol^{-1}} + 282.5\ \mathrm{kJ\ mol^{-1}} + (-69.04\ \mathrm{kJ\ mol^{-1}}) = 140.4\ \mathrm{kJ\ mol^{-1}}$$

for Ni(111) and

$$E_{ed}^{n=0}[\mathrm{Au(111)}] = -116.73\ \mathrm{kJ\ mol^{-1}} + 250\ \mathrm{kJ\ mol^{-1}} + (-25.78\ \mathrm{kJ\ mol^{-1}}) = 107.5\ \mathrm{kJ\ mol^{-1}}$$

for Au(111).

From these calculations, we can derive the difference in the energy of electrodesorption from Ni(111) and Au(111) as

$$\Delta E_{ed}^{n=0}[\mathrm{Ni(111) - Au(111)}] = 32.9\ \mathrm{kJ\ mol^{-1}}$$

In all of these calculations, we have assumed that unreconstructed Ni(111) is the predominant surface structure for the reason that the pseudosquare reconstruction dominant at room temperature[25] is related to a 163.3-eV binding energy in the XPS measurements, while SCH_3^- in a 3-fold hollow on Ni(111) has an S $2p_{3/2}$ binding energy of approximately 162.3 eV,[25] which is much closer to the 162.5 eV measured in the present work. We have used in the calculations $E_{S-s} = -69$ kJ mol^{-1} [57] rather than -50 kJ mol^{-1} [58] because the first value agrees very well with the recent DFT calculation for the adsorption of water on Rh and Pt including hydrogen bonding between the adsorbed molecules.[62]

We can now estimate the difference in electrodesorption peak potentials, $\Delta E_p^{n=0}[\mathrm{Ni(111) - Au(111)}]$, from the Ni(111) − Au(111) values. As was already discussed by Azzaroni et al.,[30] electrochemical potential differences can be assimilated to enthalpic changes because entropy contributions in the reductive electrodesorption taking place on the Au and Ni surfaces should be similar and can therefore be canceled. Considering a one-electron charge transfer (eq 7) and

$$\Delta E_{ed}^{n=0}[\mathrm{Ni(111) - Au(111)}] = 32.9\ \mathrm{kJ\ mol^{-1}}$$

we obtain

$$\Delta E_p^{n=0}[\mathrm{Ni(111) - Au(111)}] = 0.34\ \mathrm{V}$$

This difference indicates that, at a constant n (i.e., for the same number of C atoms), alkanethiolate electrodesorption from Ni should be 0.34 V more negative than the same process on the Au(111) surface. In all of these estimates, we have considered an admixture of hollow fcc and hollow hcp site occupancy. However, bridge site occupancy cannot be ruled out either from combined NIXSW and NEXAFS results[27] nor from our calculated E_{ads} values (Table 2). The resulting energy and potential differences for the less probable bridge site occupancy are

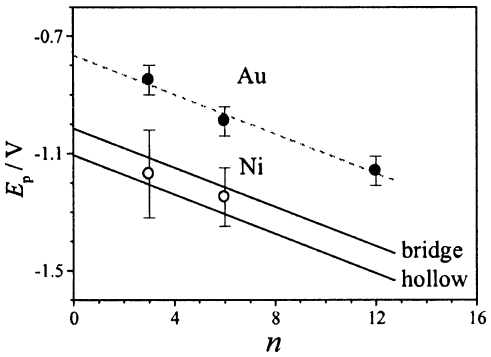

Figure 8. Calculated and measured electrodesorption peak potentials, E_p, for Au (●) and Ni (○) as a function of the aliphatic chain length, n. Data for Au were measured from voltammetric peak positions; data for Ni were estimated from Figure 7. The straight lines correspond to a linear regression with a slope of −3.5 kJ mol^{-1}, for Au, and estimates from the DFT calculations, for Ni bridge and hollow site occupancy, respectively.

$$\Delta E_{ed}^{n=0}[\mathrm{Ni(111)_{bridge} - Au(111)}] = 22.9\ \mathrm{kJ\ mol^{-1}}$$

and

$$\Delta E_p^{n=0}[\mathrm{Ni(111)_{bridge} - Au(111)}] = 0.25\ \mathrm{V}$$

These values are only indicative about the potential region where alkanethiolates should be electrodesorbed from the Ni(111) surface.

As a preliminary trial to the predicted electrodesorption potential differences, in Figure 8 we have plotted theoretical curves and E_p values for C3, C6, and C12 on Au and Ni. For Au, we have determined the peak position, E_p, directly from the respective voltammograms. Note that E_p values obtained in this work in alkanethiolate-containing 1 M NaOH are ≈0.08 V more negative than those previously reported for alkanethiolate-covered Au in plain 0.1 M NaOH.[63] The more concentrated solution and the presence of alkanethiolate molecules in the electrolyte could explain this difference. For Ni_{poly}, we have estimated the respective E_p values from the potential value at which the S signal starts to exhibit a decrease in relation to its maximum value (Figure 7). The E_p curve for Au is a linear regression through data points, with $E_p^{n=0}[\mathrm{Au(111)}] = -0.75$ V and a slope of −3.5 kJ mol^{-1} per number of C atoms. For the theoretical E_p vs n plots for Ni(111), we have used $\Delta E_p^{n=0}[\mathrm{Ni(111)_{bridge} - Au(111)}] = 0.25$ V and $\Delta E_p^{n=0}[\mathrm{Ni(111)_{hollow} - Au(111)}] = 0.34$ V. This figure clearly explains the survival of dodecanethiolates on the Ni(111) surface at $E_{ad} \leq -1.5$ V. Although it is evident that polycrystalline surfaces exhibit a large number of surface terminations, and therefore a variety of adsorption sites, so that no direct correlation should be made with the DFT calculations, values for Au(111)[30] and Cu(111)[28] have results that are consistent with those found on the respective polycrystalline surfaces. In Figure 8, the experimental values for the alkanethiolate electrodesorption from Ni_{poly} lie close to the theoretical lines for Ni(111). It is important to stress that this conclusion remains valid if other E_p values for alkanethiolate electrodesorption from Au reported in the literature for alkaline media are used.[30,63]

Finally, we can discuss the origin of the relative electrochemical stability of alkanethiolates on Ni with respect to other metals. Alkanethiolate SAMs on Ni are more stable than those formed on Au surfaces because the alkanethiolate adsorption energy is higher and the ϵ_{HOMO} smaller than the analogous energy values estimated for Au surfaces. On the other hand, despite the fact that the adsorption energy of alkanethiolates on Ni (Table 2) is higher than that estimated on Cu,[28] the ϵ_{HOMO} values for Ni are also much higher. This means that, to introduce an electron into the alkanethiolate−Cu system, much more negative potentials are required in relation to those required for the alkanethiolate−Ni system. In the final energy balance, this term predominates, explaining the higher stability of alkanethiolate SAMs on Cu against reductive electrodesorption.

5. Outlook and Conclusions

The electrochemical formation of alkanethiolate SAMs on Ni(111) and polycrystalline Ni surfaces from alkanethiol-containing aqueous 1 M NaOH solutions was studied with AES, XPS, electrochemical techniques, and DFT calculations. The main conclusions are as follows:

(i) Results for propanethiol (C3), hexanethiol (C6), and dodecanethiol (C12) show that alkanethiolates adsorb on Ni surfaces as the NiO electroreduction takes place. Therefore, in contrast to Au and Ag, alkanethiolate electroadsorption on Ni takes place at a fixed potential range, irrespective of the hydrocarbon chain length.

(ii) Electrochemical and XPS data reveal that, at room temperature, alkanethiolate electroadsorption from aqueous solutions results in the formation of a Ni−thiolate bond, contrary to what is observed for alkanethiolate adsorption from the gas phase, where S−C bond cleavage occurs at or below these temperatures.

(iii) The alkanethiolate surface coverage is dependent on the applied potential and hydrocarbon chain length. The final alkanethiolate surface coverage increases as the hydrocarbon chain length increases, approaching a full monolayer, which is stable even at very high cathodic potentials (−1.5 V vs SCE), in the case of C12.

(iv) DFT calculations show that the greater stability against electrodesorption found for alkanethiolate SAMs on Ni, with respect to SAMs on Au, is related not only to the larger alkanethiolate adsorption energy but mainly to the larger difficulty to introduce electrons in the alkanethiolate−Ni system.

(v) Electrochemical self-assembly from aqueous NaOH media saturated with alkanethiol appears as a straightforward route to building stable SAMs of long-chained alkanethiolates on Ni surfaces.

(vi) The dodecanethiolate SAMs hinder the HER, as well as the electrodissolution of Ni, in aqueous 0.1 M HCl. Therefore, dodecanethiolate SAMs on Ni are promising candidates both for corrosion protection and as intermediates for master-mold transfer.

Results from this paper open new paths for further research work. In particular, a complete characterization of alkanethiolate SAMs on Ni prepared from electrochemical self-assembly is needed. Scanning tunneling microscopy imaging of alkanethiolate SAM on Ni(111) is required to obtain local information about the surface structures and defects present in the monolayer. The SAM thickness can be investigated by ellipsometric measurements combined with atomic force microscopy. IR spectroscopy can be used to learn about the presence of order in the hydrocarbon chains and chain orientations and also to probe the presence of intact S−C bonds for SAMs prepared at high negative potentials. The behavior of dodecanethiolate SAMs in neutral and alkaline media containing chloride anions should also be investigated to evaluate their ability to protect the metal against pitting corrosion.

Acknowledgment. The authors thank Dr. Julio Esteban Gayone for his assistance with the XPS experiments and also for his useful discussions. This work was supported by the Agencia Nacional de Promoción Científica y Tecnológica (Grants PICT02-11111, -03-11799, and -03-17492) and CONICET (Grants PIP 0897 and PEI 6037) (Argentina) and Ministerio de Ciencia y Tecnología (Grant BQU2002-03249) (Spain). H.A. and G.Z. are also members of CONICET.

References and Notes

(1) Ulman, A. *Chem. Rev.* **1996**, *96*, 1533.
(2) Gates, B. D.; Xu, Q.; Stewart, M.; Ryan, D.; Willson, C. G.; Whitesides, G. M. *Chem. Rev.* **2005**, *105*, 1171.
(3) Love, J. C.; Estroff, L. A.; Kriebel, J. K.; Nuzzo, R. G.; Whitesides, G. M. *Chem. Rev.* **2005**, *105*, 1103.
(4) Wolf, S. A.; Awschalom, D. D.; Buhrman, R. A.; Daughton, J. M.; von Molnar, S.; Roukes, M. L.; Chtchelkanova, A. Y.; Treger, D. M. *Science* **2001**, *294*, 1488.
(5) Stratmann, M. *Adv. Mater*. **1990**, *29*, 191.
(6) Schilardi, P. L.; Azzaroni, O.; Salvarezza, R. C. *Langmuir* **2001**, *17*, 2747.
(7) Azzaroni, O.; Fonticelli, M.; Benítez, G.; Schilardi, P. L.; Gago, R.; Caretti, I.; Vázquez, L.; Salvarezza, R. C. *Adv. Mater.* **2004**, *16*, 405.
(8) Schreiber, F. *Prog. Surf. Sci*. **2000**, *65*, 151 and references cited therein.
(9) Widrig, C. A.; Chung, C.; Porter, M. D. *J. Electroanal. Chem.* **1991**, *310*, 335.
(10) Walczak, M.; Alves, C. A.; Lamp, B. D.; Porter, M. D. *J. Electroanal. Chem.* **1995**, *396*, 103.
(11) Zhong, C.-J.; Porter, M. D. *J. Electroanal. Chem.* **1997**, *425*, 147.
(12) Walczak, M. M.; Chung, C.; Stole, S. M.; Widrig, C. A.; Porter, M. D. *J. Am. Chem. Soc.* **1991**, *113*, 2370.
(13) Hatchett, D. W.; White, H. S. *J. Phys. Chem.* **1996**, *100*, 9864.
(14) Hatchett, D. W.; Stevenson, K. J.; Lacy, W. B.; Harris, J. M.; White, H. S. *J. Am. Chem. Soc*. **1997**, *119*, 6596.
(15) Hatchett, D. W.; Uibel, R. H.; Stevenson, K. J.; Harris, J. M.; White, H. S. *J. Am. Chem. Soc*. **1998**, *120*, 1062.
(16) Ron, H.; Cohen, H.; Matlis, S.; Rubinstein, I. *J. Phys.Chem. B* **1998**, *102*, 986115.
(17) Himmelhaus, M.; Gauss, I.; Buck, M.; Eisert, F.; Wöll, C.; Grunze, M. *J. Electron Spectrosc. Relat. Phenom.* **1998**, *92*, 139.
(18) Ziegler, K. J.; Doty, R. C.; Johnston, K. P.; Korgel, B. A. *J. Am. Chem. Soc*. **2001**, *123*, 7797.
(19) Mekhalif, Z.; Riga, J.; Pireaux, J. J.; Delhalle, J. *Langmuir* **1997**, *13*, 2285.
(20) Noël, S.; Houzé, F.; Boyer, L.; Mekhalif, Z.; Delhalle, J.; Caucano, R. *IEEE Trans. Compon. Packag. Technol.* **1999**, *22*, 79.
(21) Mekhalif, Z.; Laffineur, F.; Couturier, N.; Delhalle, J. *Langmuir* **2003**, *19*, 637.
(22) Morin, D. *J. Electroanal. Chem.* **2004**, *565*, 235.
(23) Jackson, G. J.; Woodruff, D. P.; Jones, R. G.; Singh, N. K.; Chan, A. S. Y.; Cowie, B. C. C.; Formoso, V. *Phys. Rev. Lett.* **2000**, *84*, 119.
(24) Castro, M. E.; White, J. M. *Surf. Sci.* **1991**, *257*, 22.
(25) Rufael, T. S.; Huntley, D. R.; Mullins, D. R.; Gland, J. L. *J. Phys. Chem. B* **1998**, *102*, 3431.
(26) Mullins, D. R.; Tang, T.; Chen, X.; Sneerson, V.; Saldin, D. K.; Tysoe, W. T. *Surf. Sci.* **1997**, *372*, 193.
(27) Fisher, C. J.; Woodruff, D. P.; Jones, R. G.; Cowie, B. C. C.; Formoso, V. *Surf. Sci*. **2002**, *496*, 73.
(28) Azzaroni, O.; Vela, M. E.; Fonticelli, M.; Benítez, G.; Carro, P.; Blum, B.; Salvarezza, R. C. *J. Phys. Chem. B* **2003**, *107*, 13446.
(29) Kakiuchi, T.; Usui, H.; Hobara, D.; Yamamoto, M. *Langmuir* **2002**, *18*, 5231.
(30) Azzaroni, O.; Vela, M. E.; Andreasen, G.; Carro, P.; Salvarezza, R. C. *J. Phys. Chem. B* **2002**, *106*, 12267.
(31) Byloos, M.; Al-Maznai, H.; Morin, M. *J. Phys. Chem. B* **1999**, *103*, 6554.
(32) Danckwerts, M.; Savinova, E.; Pettinger, B.; Doblhofer, K. *Appl. Phys. B* **2002**, *74*, 635.
(33) Becke, A. D. *J. Chem. Phys*. **1993**, *98*, 5648.
(34) Hay, P.; Wadt, R. *J. Chem. Phys.* **1985**, *82*, 299.
(35) Levine, I. N. *Quantum Chemistry*, 5th ed.; Prentice Hall: Englewood Cliffs, NJ, 2000; p 492.

(36) Morin, C.; Eichler, A.; Hirschl, R.; Sautet, P.; Hafner, J. *Surf. Sci.* **2003**, *540*, 474.
(37) Frish, M.; et al. *Gaussian98W*; Gaussian Inc.: Pittsburgh, PA, 1998.
(38) Emsley, J. *The Elements*; Clarendon Press: Oxford, U.K., 1989; p 124.
(39) Machado, A. S. S.; Avaca, L. *Electrochim. Acta* **1994**, *10*, 1385.
(40) Davis, L. E.; MacDonald, M. C.; Palmberg, P. W.; Riach, G. E.; Weber, R. E. *Handbook of Auger Electron Spectroscopy*, 2nd ed.; Physical Electronic Industries Inc.: Eden Prairie, MN, 1976.
(41) Jablonski, A.; Powell, C. J. *Surf. Sci. Rep.* **2002**, *47*, 33−91.
(42) Laibinis, P. E.; Bain, C. D.; Whitesides, G. M. *J. Phys. Chem.* **1991**, *95*, 7017.
(43) Marcus, P. *Electrochim. Acta* **1998**, *43*, 109.
(44) Moulder, J. F.; Sticle, W. F.; Sobol, P. E.; Bomben, K. D. *Handbook of X-ray Photoelectron Spectroscopy*; Physical Electronics: Eden Prairie, MN, 1995.
(45) Love, J. C.; Wolfe, D. B.; Haasch, R.; Chabinyc, N. L.; Paul, K. E.; Whitesides, G. M.; Nuzzo, R. G. *J. Am. Chem. Soc.* **2003**, *125*, 2597.
(46) Yu, X.-R.; Liu, F.; Wang, Z.-Y.; Chen, Y. *J. Electron Spectrosc.* **1990**, *50*, 159.
(47) van der Heide, H.; Hemmel, R.; van Bruggen, C. F.; Haas, C. *J. Solid State Chem.* **1980**, *33*, 17.
(48) Vogt, A. D.; Han, T.; Beebe, T. P., Jr. *Langmuir* **1997**, *13*, 3397.
(49) Adams, D. M.; Brus, L.; Chidsey, C. E. D.; Creager, S.; Creutz, C.; Kagan, C. R.; Kamat, P. V.; Lieberman, X. M.; Lindsay, O. S.; Marcus, R. A.; Metzger, R. M.; Michel-Beyerle, M. E.; Miller, J. R.; Newton, M. D.; Rolison, D. R.; Sankey, O.; Schanze, K. S.; Yardley, J.; Zhu, S. *J. Phys. Chem. B* **2003**, *107*, 6668.
(50) Han, Q.; Liu, K.; Li, X.; Wei, X. *Int. J. Hydrogen Energy* **2004**, *29*, 243.
(51) Gonsalez, E. R.; Avaca, L. A.; Tremiliosi-Filho, G.; Machado, S. A. S.; Ferreira, M. *Int. J. Hydrogen Energy* **1994**, *19*, 17.
(52) Perdereau, M.; Oudar, J. *Surf. Sci*. **1970**, *20*, 80.
(53) Paredes Olivera, P.; Patrito, E. M.; Sellers, H. *Surf. Sci.* **1998**, *418*, 376.
(54) Vericat, C.; Andreasen, G.; Vela, M. E.; Martin, H.; Salvarezza, R. C. *J. Chem. Phys*. **2001**, *115*, 6672.
(55) Singh, R.; Whitesides, G. M. In *Supplement S: The Chemistry of Sulphur-Containing Functional Groups*; Patai, S., Rappoport, Z., Eds.; John Wiley and Sons: New York, 1993.
(56) Benítez, G.; Vericat, C.; Tanco, S.; Remes Lenicov, F.; Castez, M. F.; Vela, M. E.; Salvarezza, R. C. *Langmuir* **2004**, *20*, 5030.
(57) Paredes Olivera, P.; Patrito, E. M.; Sellers, H. *Surf. Sci.* **1995**, *327*, 330.
(58) Sebastiani, D.; Delle Site, L. *J. Chem. Theory Comput.* **2005**, *1*, 78.
(59) Sexton, B. A.; Hughes, A. E. *Surf. Sci.* **1984**, *140*, 227.
(60) Chong, D. P.; Gritsenko, O. V.; Baerends, E. J. *J. Chem. Phys.* **2002**, *116*, 1760.
(61) Yang, H.; Caves, T. C.; Whitten, J. L.; Huntley, D. R. *J. Am. Chem. Soc.* **1994**, *116*, 8200.
(62) Vassilev, P.; van Santen, R. A.; Koper, M. T. M. *J. Chem. Phys.* **2005**, *122*, 054701.
(63) Vela, M. E.; Martin, H.; Vericat, C.; Andreasen, G.; Hernández-Creus, A.; Salvarezza, R. C. *J. Phys. Chem. B* **2000**, *104*, 11878.